Progress In Electromagnetics Research, Vol. 115, 11–33, 2011

KINEMATIC PROPERTIES OF SHORT-PULSED SPARSE TRANSMITTING ARRAYS

A. Shlivinski

Department of Electrical and Computer Engineering
Ben-Gurion University of the Negev
Beer-Sheva 84105, Israel

Abstract—The kinematic properties of an array of transmitting antennas that are transiently excited by a sequence of modulated pulses, with high repetition rate, are explored. The array's parameterization is carried out via the energy radiation pattern. It is shown that the energy radiation pattern can be decomposed into a set of different types of beam contributions, defined over a beam-skeleton, which is determined by the array's physical and excitation parameters. The different types of beams are main beams, grating-lobe beams and cross-pulsed lobe beams, each corresponding to a different pulsed interference mechanism. While grating lobes are time-harmonic phenomena, cross-pulsed lobes are unique for excitation with a pulsed sequence. The different beam types set limits for array sparsity in terms of the array's physical and excitation parameters. The array's directivity is introduced as a figure of merit of its performance and to demonstrate the resulting effect of the time-domain excitation characteristics. The array's parameterization can be used with any type of excitation — from extreme narrow band (time-harmonic) to extreme ultra-wideband (transient/short pulsed) excitation. For time-harmonic excitation, the resulting characterization matches that of the classical frequency domain antenna theory.

1. INTRODUCTION

The ever increasing signal bandwidth of transmit/receive systems, ranging from narrow-band (NB) to ultra-wideband (UWB) regimes or alternatively from time-harmonic (TH) to transient/short-pulsed (SP)

Received 9 February 2011, Accepted 16 March 2011, Scheduled 17 March 2011
Corresponding author: Amir Shlivinski (amirshli@ee.bgu.ac.il).

regimes, has led to the formulation of radiation concepts for time-dependent signals in both electromagnetics and acoustics directly in the time domain (TD) [1–4]. Of particular interest is the application of UWB/SP signals as excitations to an antenna array and the effect of these signals on the array's performance (and synthesis). The fundamental theory governing single TD radiating elements has previously been addressed (see, e.g., [1, 5–7]), as has the case of an array fed by pulsed [1, 8–25].

This paper explores the fundamental kinematic aspects of a periodic true time delay (TTD) beam steering array under excitation of a finite sequence of modulated pulses with, possibly, HPRF (high pulsed repetition frequency). While the kinematic properties of single pulse excitation have been extensively discussed (see, e.g., [9, 13, 18, 23]), only scant attention has been given to the HPRF case [15]. The motivation for exploring the HPRF case follows from its profound effect on the radiation pattern, whether the time-dependent pattern or the associated energy pattern. This HPRF effect can be found in the introduction of a new type of beams termed cross-pulsed lobe (CPL) beams in addition to the main radiation beam (in the array steering direction) and the grating lobes (GL). These CPL beams occur as a result of the interaction of differently tagged pulses radiated from different elements of the array, see, e.g., [15]. As for GLs in the TH case (see, e.g., [13, 24] for the single pulse excitation), the CPLs set bound on the array's performance. Moreover, CPLs, also, set restrictions on the sparsity of the array to meet CPL-free radiation pattern. These restrictions become important when the array is used, for example, in remote-sensing/imaging systems in which additional radiated "spurious" beams (CPL) may degrade the overall performance. This contribution is aimed to extend the mathematical formulation of these kinematic properties by providing an extensive analysis and quantification followed by demonstrations of these concepts in view of the energy radiation pattern.

The paper is organized as follows: Problem formulation is given in Section 2. The array pattern is set in Section 3 as the basic observable quantity for further characterization. The presentation in Section 3 is motivated by the configuration of the TTD array, however, similar discussion can also be use for other array applications. A detailed derivation and array characterization is further given in Section 4 by the beam skeleton and in Section 5 by the beam summation decomposition. The array sparsity is elaborated in Section 6 by introducing alternative sparsity measures to meet some GL and CPL–free radiation patterns. The array directivity is discussed in Section 7 in the light of the beam skeleton structure, sparsity, and array

parameters. The discussion is followed by numerical simulations to demonstrate the discussed concepts. A concluding section is given in Section 8.

2. PROBLEM FORMULATION

In the following section the problem formulation is presented in terms of the radiating array layout, the model of the array's elements, and the observation setup.

2.1. UWB/SP Array and Excitation Setup

Let us consider a one-dimensional linear array of N radiating elements aligned along the z axis with inter-element spacing d. Without loss of generality, all array elements have the same source-to-far-field transfer function (termed effective height) $\mathbf{h}^t(\hat{\mathbf{r}}, t)$, where t is a temporal coordinate, $\hat{\mathbf{r}} = (v\boldsymbol{\rho}, u)$ with $\boldsymbol{\rho} = \hat{\mathbf{x}}\cos\phi + \hat{\mathbf{y}}\sin\phi$, $u = \cos\theta$ and $v = \sin\theta$, $0 \leq \theta \leq \pi$, $0 \leq \phi \leq 2\pi$. In the present discussion, we consider radiating elements having $\mathbf{h}^t(\hat{\mathbf{r}}, t) = \mathbf{f}(\hat{\mathbf{r}})D(t)$, where $\mathbf{f}(\hat{\mathbf{r}})$ is an angular vectorial radiation pattern in the $\hat{\mathbf{r}}$ direction and $D(t)$ is a temporal operator. This decomposition of $\mathbf{h}^t$ as a product of temporal and spectral functions mathematically describes many types of small antennas having a multipolar type of radiation pattern with $D(t)$ a differential operator (see, e.g., in antenna theory [9, 23, 26]). For extended type of antennas, $\mathbf{h}^t(\hat{\mathbf{r}}, t)$ can be decomposed as a combination of products of spectral and temporal functions (see, e.g., [27]). Additionally, the array is set such that the main radiation beam is steered into the $\hat{\mathbf{r}}_0 = (\sin\theta_0, 0, \cos\theta_0)$ direction (note that since the one-dimensional array is aligned along the z direction, it is not applicable to steer the beam in the ϕ direction).

Let us also assume that at the terminal of each of the radiating elements the incident excitation signal $s(t)$ is a sequence of M pulse-shaped waveforms $s_0(t)$:

$$s(t) = \sum_{m=0}^{M-1} s_0(t - mT_p), \tag{1}$$

where T_p is the pulse repetition duration (with PRF $= T_p^{-1}$), and $s_0(t)$ is an essentially time and frequency band-limited pulse-shaped waveform with a prescribed central frequency T_0^{-1} (T_0 is the period of the signal, see the discussion below).

Combining the excitation model in (1) with the radiating elements model, the single element's (far field) transient radiation pattern is

given by [7]:

$$\mathbf{e}(\hat{\mathbf{r}},t)=\frac{1}{4\pi r}\left[\mathbf{h}^t(\hat{\mathbf{r}},\cdot)\circledast s(\cdot)\right](\tau)=\frac{1}{4\pi r}\sum_{m=0}^{M-1}\mathbf{f}(\hat{\mathbf{r}})e_0(\tau-mT_p), \quad (2a)$$

with the pulsed waveform

$$e_0(\tau)=[D(\cdot)\circledast s_0(\cdot)](\tau), \quad (2b)$$

where $\mathbf{r}=(x,y,z)$, with $r=|\mathbf{r}|$, the retarded time $\tau=t-r/c$, c is the wave propagation speed, and $[a(\cdot)\circledast b(\cdot)](t)=\int dt' a(t')b(t-t')$ is the convolution integral. In view of (2a), the element's far-field waveform $e_0(\tau)$ is also a pulsed waveform that has some pulsed characteristics, which due to $D(t)$ differ from those of its source $s_0(t)$.

Since $D(t)$ may contain derivations and since $s_0(t)$ has a pulsed shape, it follows from (2b) that $e_0(\tau)$ may be modeled (approximated) as a modulated pulsed-waveform. Consequently, for purposes of modelling and for the sake of simplicity, let $e_0(t)=r_0(t)\cos(\omega_0 t)$, where $r_0(t)$ is a base-band pulse shaped window with an effective pulse-width, say, T[†], and $\omega_0=2\pi/T_0$ is the radian frequency of the carrier. Note that $cT_0=\lambda_0$, where $\lambda_0=2\pi c/\omega_0$ is the wavelength at ω_0. The ratio T/T_0 approximates the number of cycles contained under the pulsed envelope (r_0). As such it is related to the signal's frequency bandwidth, therefore it can be used for the classification of the "pulsed excitation" into one of three types: (*i*) NB for $T/T_0\gtrsim\mathcal{O}(1)$, i.e., $\omega_0 T>\mathcal{O}(1)$, where the signal is dominantly characterized by the carrier frequency-ω_0 [thus TH (frequency domain) considerations may be used]; (*ii*) UWB/SP for $T/T_0\lesssim 0.2$, i.e., $\omega_0 T\lesssim 1$, where the signal is dominated by the short pulsed envelope (window); or (*iii*) the intermediate range of $0.2\lesssim T/T_0\lesssim 1$, termed the quasi-monochromatic (QM) regime, where the signal's characteristics are obtained as an interplay between NB (carrier) and UWB/SP (modulation) properties. Thus modeling $e_0(t)$ as a modulated pulse allows for a unified quantification of some unique kinematic properties that are attributed to QM and UWB/SP excitation regimes.

The distinction between the excitation regimes implies that the inter-element spacing should also be normalized differently in each of the regimes in accordance with the dominant parameter that characterizes the signal. To this end, in the NB regime the normalization should be carried out with respect to the carrier period: $d/cT_0=d/\lambda_0$ (note that this normalization is the one traditionally used in TH antenna theory). On the other hand, in the UWB/SP regime the normalization should be carried out with respect to the

[†] The pulse-width T can be approximated by $T\sim\|te_0(t)\|_2/\|e_0\|_2$, where $\|\,\|_2$ is the $\mathcal{L}_2$ norm that is used in (3) [15].

pulse width: d/cT (note that this normalization may, unnaturally, be written in terms of the carrier wavelength $(d/\lambda_0)(T/T_0)^{-1}$ even though for UWB/SP, due to their extreme bandwidth, it is difficult to physically interpret the wavelength of the signal). In the intermediate, QM, regime there is no single dominant signal parameter that can be used, conveniently, to normalize d.

2.2. Observable Quantities

As we did for to the element's far-field in (2a), let us assume that the array's time-dependent far-field is given by $\mathbf{E}(\mathbf{r},t) = \frac{1}{4\pi r}\mathbf{F}(\hat{\mathbf{r}},\tau)$, where $\mathbf{F}(\hat{\mathbf{r}},\tau)$ is the corresponding radiation pattern (see the discussion below). Since the kinematic properties of the array with respect to its energy radiation characteristics are of concern in this paper, the main observable quantity to be used is the array's energy radiation pattern $\mathcal{E}(\hat{\mathbf{r}})$, which is defined via the $\mathcal{L}_2$ norm as,

$$\mathcal{E}(\hat{\mathbf{r}}) = (4\pi r)^2 \left\|\mathbf{E}(\mathbf{r},t)\right\|_2^2 = \int_\infty d\tau \left|\mathbf{F}(\hat{\mathbf{r}},\tau)\right|^2. \tag{3}$$

As will be shown below it is convenient to represent energy quantities via an autocorrelation function. To this end, $\mathcal{E}(\hat{\mathbf{r}})$ in Eq. (3) is given by $\mathcal{E}(\hat{\mathbf{r}}) = \mathcal{R}_F(\tau;\hat{\mathbf{r}})|_{\tau=0}$, where the temporal autocorrelation function is given by:

$$\mathcal{R}_F(\tau;\hat{\mathbf{r}}) = \mathbf{F}(\hat{\mathbf{r}},\tau) \star \mathbf{F}(\hat{\mathbf{r}},-\tau) = \int_\infty dt\, \mathbf{F}(\hat{\mathbf{r}},t+\tau/2)\cdot\mathbf{F}(\hat{\mathbf{r}},t-\tau/2), \tag{4}$$

where, here, $\star$ is identified as scalar product and convolution, and $\cdot$ indicates a scalar product.

It should be noted that Eq. (3) may also be interpreted within a transmit-receive relation, where the receiving antenna is a fictitious field-sampling space-time point-like probe, which is located in the far-zone of the array. Therefore, $\mathcal{E}(\hat{\mathbf{r}})$ represents the total energy received at the probe's terminals. For more realistic probes a Friis-type relation for the calculation of $\mathcal{E}(\hat{\mathbf{r}})$ should be used [7].

3. ARRAY PATTERN

Following the formulation in Section 2, the array radiation pattern will be presented next as the main analysis tool.

Assuming that each of the radiating elements is insonified by $s(t)$ of (1) to yield the radiated field $\mathbf{e}(\hat{\mathbf{r}},\tau)$ of (2a), the time-dependent array's radiation pattern $\mathbf{F}(\hat{\mathbf{r}},\tau)$ is obtained by delaying the elements' contributions by two progressive delay terms: the spatial

delay $dc^{-1}\cos\theta$ and the steering delay $t_d = dc^{-1}\cos\theta_0$, which aims to steer the main radiation beam into the $\hat{\mathbf{r}}_0$ direction, thus giving:

$$\mathbf{F}(\hat{\mathbf{r}},\tau) = \mathbf{f}(\hat{\mathbf{r}})F_a(\hat{\mathbf{r}},\tau),\ F_a(\hat{\mathbf{r}},\tau) = \sum_{n=0}^{N-1}\sum_{m=0}^{M-1} e_0\left(\tau + ndc^{-1}\cos\theta - nt_d - mT_p\right). \tag{5}$$

Note that $F_a(\hat{\mathbf{r}},\tau)$ may be regarded as the radiation pattern of the array itself without the spectral "filtering" effect of the elements' angular pattern. The discussion here is directed toward the analysis of the array's kinematic properties, and therefore inter-element coupling is neglected. Note though that in TD transient array analysis inter-element coupling is manifested as a weak delayed-type response (see, e.g., [23]).

Inserting Eqs. (5) and (1) into Eq. (3) yields the expression for the energy radiation pattern, which may be rearranged as:

$$\mathcal{E}(\hat{\mathbf{r}}) = |\mathbf{f}(\hat{\mathbf{r}})|^2\mathcal{E}_a(\hat{\mathbf{r}}), \qquad \mathcal{E}_a(\hat{\mathbf{r}}) = \mathcal{R}_{F_a}(0;\hat{\mathbf{r}}), \tag{6a}$$

where $\mathcal{R}_{F_a}$ is the autocorrelation of F_a, which is given by the expression in (4) but for F_a (instead of F), giving:

$$\mathcal{E}_a(\hat{\mathbf{r}}) = \mathcal{E}_a(u) = \sum_{n=0}^{N-1}\sum_{m=0}^{M-1}\sum_{k=0}^{N-1}\sum_{l=0}^{M-1}\mathcal{R}\left[c^{-1}d(n-k)(u-u_0) - (m-l)T_p\right], \tag{6b}$$

where $u = \cos\theta$, $u_0 = \cos\theta_0$ is a spectral variable that is restricted to $|u| \le 1$ in the visible/propagating domain, whereas $|u| \ge 1$ corresponds to the evanescent spectral domain. $\mathcal{R}(\cdot)$ is the autocorrelation function of $e_0(t)$, which is given as in (4) but with e_0. In view of (2b),

$$\mathcal{R}(\tau) = \left[\mathcal{R}_D(\cdot) \circledast \mathcal{R}_{s_0}(\cdot)\right](\tau), \tag{7}$$

in which $\mathcal{R}_{s_0}$ is the autocorrelation of the excitation pulse $s_0(t)$, and $\mathcal{R}_D(\tau) = D(\tau) \circledast D(-\tau)$ is the corresponding autocorrelation differential operator associated with $D(t)$ [‡].

To conclude, note the following: (i) The energy radiation pattern, as defined in Eq. (6a), and the array pattern F_a in Eq. (5) facilitate a general pattern multiplication principle for all excitation regimes similar to the known pattern multiplication principle for TH (or NB) excitations, see in [30, 31]; therefore justifying the identification of $\mathcal{E}_a(\hat{\mathbf{r}})$ as the array's energy pattern. (ii) $\mathcal{E}_a$ is a property of the array's physical layout, the excitation pulse ($s_0(t)$) and elements' transfer

[‡] For multipolar type of antennas, $D(t) = \delta^{(\nu)}(t)$, i.e., ν times differentiation of Dirac's delta (ν an integer, see in [7, 26, 28, 29). Therefore in Eqs. (6)–(7), the differential operator is $\mathcal{R}_D(\tau) = D(\tau) \circledast D(-\tau) = (-1)^\nu\delta^{(2\nu)}(\tau)$, giving $\mathcal{R}(\tau) = (-1)^\nu\mathcal{R}_{s_0}^{(2\nu)}$. These types of operators are employed to bring the single antenna's temporal effect into the analysis.

function ($D(t)$) manifested via $\mathcal{R}_D$. Consequently, $\mathcal{E}_a$ is the equivalent of the "array factor" that is used in TH analysis.

As stated above, the aim of this paper is to investigate the kinematic properties of the array. Following the pattern multiplication principle demonstrated by Eq. (6), the kinematic properties of the array can be recovered by treating $\mathcal{E}_a(\hat{\mathbf{r}})$. Though the expression for $\mathcal{E}_a(\hat{\mathbf{r}})$ in Eq. (6b) is inconvenient for characterization of the array's kinematic properties, it is used as the starting point for the parameterization in Section 4. It should be noted that the general line of derivation of the array radiation pattern performed in this section to yield Eq. (6) is not unique to UWB/SP TTD antenna array theory and can be found in other disciplines that employ arrays of transducers for transmission and/or reception of signals with some energy measures (see, e.g., [32, 33]). However, the present line of derivation is motivated by the use of *transient antennas with a given transient effective height*. Hence, it serves as a starting point for the discussion conducted in the next sections to derive the beam structure and other kinematic properties of such TTD arrays.

4. ARRAY ENERGY PATTERN: BEAM SKELETON

In this section, we explore the fine details of the array's energy radiation pattern $\mathcal{E}_a$ as a function of the spectral variable u. We start by deriving the beam (radiation lobes) skeleton as a set of angular directions for which $\mathcal{E}_a(u)$ has local maxima (i.e., radiation lobes) and follow by providing a TD (transient) interpretation.

4.1. Beam Skeleton Via the Energy Pattern

A possible local maximum of $\mathcal{E}_a(u)$ can be found whenever an element of the summation in Eq. (6b) reaches a local maximum as a function of u. Whether this possible local maximum can be observed in $\mathcal{E}_a(u)$, and can thus be an actual local maximum, depends both on the number of contributing summation elements that reach a local maximum at that same u and on the array parameters (of the physical layout, exciting signal, and the element's temporal response). To parametrize the angular location of the local maxima, let τ_γ with $\gamma = 0, \pm 1, \pm 2, \ldots$ such that $|\tau_0| < |\tau_{\pm 1}| < |\tau_{\pm 2}| < \ldots < \mathcal{O}(T)$ be the set of values for which $\mathcal{R}(\tau)$ obtains a local maximum (i.e., $\mathcal{R}^{(1)}(\tau_\gamma) = 0$ and $\mathcal{R}^{(2)}(\tau_\gamma) < 0$). Since $\mathcal{R}(\tau)$ is an autocorrelation function, it reaches its global maximum for $\tau = 0$; therefore, let $\tau_0 = 0$ ($\gamma = 0$). Furthermore, $\mathcal{R}(\tau) = \mathcal{R}(-\tau)$, giving $\tau_\gamma = -\tau_{-\gamma}$ ($|\gamma| \geq 1$). Thus, applying these properties of the autocorrelation function together with (6b) yields

the set of directions $u_{\alpha,\beta}$ for which $\mathcal{E}_a(u)$ obtains a local maximum:

$$u_{\alpha,\beta,\gamma} = u_{\alpha,\beta} + \frac{1}{\alpha}\left(\frac{c\tau_\gamma}{d}\right), \quad u_{\alpha,\beta} = u_{\alpha,\beta,\gamma=0} = u_0 + \left(\frac{\beta}{\alpha}\right)\left(\frac{cT_p}{d}\right) \quad (8a)$$

where α and β are integer numbers with:

$$1 \le |\alpha| \le N-1, \qquad 0 \le |\beta| \le (M-1), \qquad \gcd(\alpha,\beta) = 1. \quad (8b)$$

Note that: (*i*) As pointed out above, $u_{\alpha,\beta}$ is independent of the actual excitation signal or antenna type, since it is related to the global maximum of $\mathcal{R}(\tau)$ that is obtained for $\tau = \tau_0 = 0$. Furthermore, in light of Eq. (8a), $u_{\alpha,\beta}$ depends only on the array layout and the pulsed sequence properties (T_p, M) and not on the actual pulse shape; therefore, it is strictly a property of the array itself and may thus be identified as the beam skeleton of the array. (*ii*) Since $e_0(t)$ may contain some microstructure (such as modulation, see, e.g., its modeling in Section 2.1), its autocorrelation function $\mathcal{R}(\tau)$ may also have additional local maxima $u_{\alpha,\beta,\gamma}$ for $\tau = \tau_\gamma \neq 0$, with $\gamma \neq 0$, which depends on the pulsed-waveform and the type of antenna element. However, since $\mathcal{R}(\tau_\gamma) \le \mathcal{R}(0)$, it follows that $\mathcal{E}_a(u_{\alpha,\beta,\gamma}) \le \mathcal{E}_a(u_{\alpha,\beta,0})$, where equality is obtained for a periodic $\mathcal{R}(\tau)$ (i.e., TH excitation). Consequently, the radiation pattern attains two types of local maxima: those that depend on the periodicity of the array and the excitation pulsed sequence ($u_{\alpha,\beta}$) and those that depend on the waveform characteristics ($u_{\alpha,\beta,\gamma}$). The interpretation of these results in terms $F_a(\hat{\mathbf{r}},\tau)$ are discussed next.

4.2. Beam Skeleton Interpretation Via the Transient Pattern

The set of local maximum directions $u_{\alpha,\beta,\gamma}$ can be interpreted as being associated with different mechanisms of constructive pulsed interference [15]. The field radiation pattern at a given $u_{\alpha,\beta,\gamma}$ is obtained via Eq. (5):

$$F_a(u_{\alpha,\beta,\gamma},\tau) = \sum_{n=0}^{N-1}\sum_{m=0}^{M-1} e_0\left(\tau + \left(n\frac{\beta}{\alpha} - m\right)T_p + n\frac{1}{\alpha}\tau_\gamma\right). \quad (9)$$

From Eq. (9), two interference mechanisms are identified:

(i) Given $\alpha = n_1 - n_2$ and $\beta = m_1 - m_2$, where $0 \le n_{1,2} \le N-1$ and $0 \le m_{1,2} \le M-1$, $\gamma = 0$, $u_{\alpha,\beta} = u_{\alpha,\beta,0}$ is the direction of a complete constructive interference between pulse number m_1 radiated by element number n_1 and pulse number m_2 radiated by element number n_2; see also in of Ref. [15, Figure 2]. These local maxima (in $\mathcal{E}_a$ or more generally in $\mathcal{E}$, provided that the element's main beam pattern, $|\mathbf{f}(\hat{\mathbf{r}})|$, is wide enough) are termed CPLs. The set of CPL directions is therefore given by the beam

skeleton $\{u_{\alpha,\beta}\}$ of the radiation pattern. Note that: (i) the local maxima of the field due to cross–pulse interference result from the inherent periodicity in the array's layout and the pulsed sequence excitation; and (ii) the set of CPL directions are confined within $u_{1,-|M-1|} \leq u \leq u_{1,M-1}$. Nevertheless, the visible observation domain, $|u| \leq 1$, does not confine the contributing CPLs to $|u_{\alpha,\beta}| \leq 1$, since around each CPL direction there is a radiation lobe with some spectral content (say $\Delta_{\alpha,\beta}$). Therefore, the contributing CPLs are those with $|u_{\alpha,\beta}| \leq 1+\Delta_{\alpha,\beta}$; see also Fig. 1.

(ii) For a given α, β, as in item (i), and $\gamma \neq 0$, $u_{\alpha,\beta,\gamma}$ is the direction in which there is constructive interference of at least two contributions with a relative delay of τ_γ. However, since $\mathcal{R}(\tau) \leq \mathcal{R}(0)$, the two pulses do not overlap completely. To interpret $u_{\alpha,\beta,\gamma}$, recall the element's field modeling $e_0(t) = r(t)\cos(\omega_0 t)$ (see, Section 2.1). In the QM and NB regimes, $\mathcal{R}(\tau) \approx \frac{1}{2}R_r(\tau)\cos(\omega_0\tau)$, where $\mathcal{R}_r(\tau)$ is the autocorrelation of $r(t)$. In these frequency regimes, it follows that $\tau_\gamma \simeq \gamma T_0$. Thus, inserting $u_{\alpha,\beta,\gamma}$ into Eq. (9) suggests that the phase difference between the two interfering pulses is $\omega_0\tau_\gamma = 2\pi\gamma$, which further suggests that in the TH regime $u_{\alpha,\beta,\gamma}$ ($\gamma \neq 0$) corresponds to a GL of order γ associated with a CPL that is identified by its α, β index. Applying the above TH GL interpretation for the QM and NB excitation regimes suggests that $u_{\alpha,\beta,\gamma}$ may also be recognized as the direction in which a GL occurs. Note, however, that for $\gamma \neq 0$, the actual maxima in $\mathcal{E}_a$ are slightly perturbed from the $u_{\alpha,\beta,\gamma}$ direction due an interplay between the decaying envelop of $\mathcal{R}_r(\tau)$ and the peak of the cosine modulating term in $\mathcal{R}(\tau)$. The major difference between the TH regime and the QM and NB regimes is that since $\mathcal{R}(\tau_\gamma) \leq \mathcal{R}(0)$, the GLs' peak magnitudes in QM and NB decay as $|\gamma|$ increases.

Finally, we should note that for the NB and extreme QM excitation regimes, side lobes (SLs) can also be observed. SLs are formed via an interference mechanism similar to the mechanism that gives rise to GLs, but with a relative delay between any two interfering contributions, which is a fraction of τ_γ, with an additional constraint over the total delay between the earliest and latest pulsed contributions. Further parameterization of SLs will not be pursued here, since they are of negligible magnitude for QM and UWB/SP types of excitation due to difficulties in achieving a complete constructing/destructing interference as a result of the pulsed shape of the waveform.

4.3. Beam Skeleton Example

To conclude the discussion in this section, we provide an example to demonstrate the above concepts of the energy radiation pattern and beam skeleton.

In this example (Fig. 1), the energy radiation pattern is depicted for a sparse array of $N = 7$ omnidirectional point-like radiating elements with an inter-element spacing of $d/cT = 50$, and $u_0 = 0$. The excitation is set to yield a pulsed wave-field that can be modeled as a sequence of $M = 15$ Gaussian modulated pulses $e_0(t) = r(t)\cos\omega_0(t)$ (see Section 4.2 item ii) with $r(t) = e^{-\frac{1}{2}(t/T)^2}$ and $T_p/T = 45$. Figs. 1(a) and 1(b) depict $\mathcal{E}_a$ for two carrier frequencies, an UWB/SP signal with $T/T_0 = 0.1$ and a QM excitation signal with $T/T_0 = 0.5$ (recall that the frequency regime of the excitation signal is dictated by T/T_0, where T_0 is used for nornalization). The CPLs are clearly visible at the local maxima for $0 < |u| \leq 1$. Table 1 lists the CPLs' central angular locations ($u_{\alpha,\beta}$ calculated by (8a) with $\gamma = 0$) and their associated relative level of magnitudes (array CPL level, A-CPLL, see in Section 5). Note that in Fig. 1(b), QM excitation, the $\gamma = \pm 1$ GLs associated with each CPL can be seen by the additional peaks around each of the CPLs.

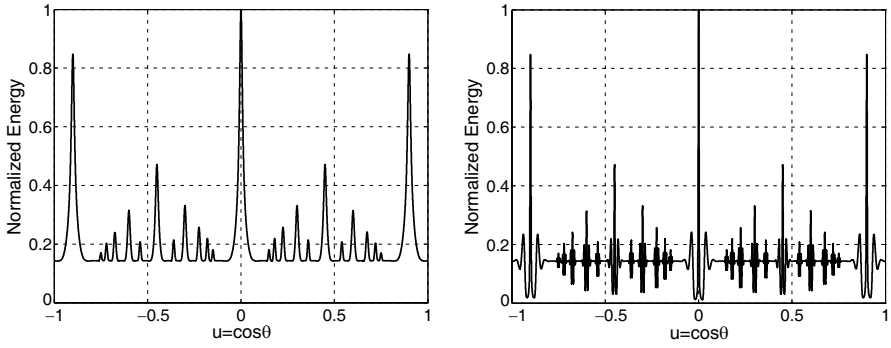

Figure 1. Energy radiation pattern $\mathcal{E}$ for a sparse array of $N = 7$ omnidirectional radiating elements with inter-element spacing $d/cT = 50$ excited by a sequence of $M = 15$ pulses that can be modeled by Gaussian modulated pulses and $T_p/T = 45$, (a) $T/T_0 = 0.1$ (UWB/SP); and (b) $T/T_0 = 0.5$ (QM).

Table 1. Central angular location of the CPLs.

α	β	$\pm u_{\alpha,\beta}$ (Eq. (8))	A-CPLL (Eq. (11))
1	1	0.9	0.8476
2	1	0.45	0.4721
3	1	0.3	0.3306
3	2	0.6	0.3143
4	1	0.225	0.2571
4	3	0.675	0.2408
5	1	0.18	0.2190
5	2	0.36	0.2136
5	3	0.54	0.2082
5	4	0.72	0.2027
6	1	0.15	0.1810
6	5	0.75	0.1701

5. ARRAY PATTERN: BEAM SUMMATION

Having defined the beam skeleton in Section 4, we now reformulate the summation in Eq. (6b) as a summation of beam contributions[§] that are structured upon the CPL beam skeleton $\{u_{\alpha,\beta}\}$. To this end, let the energy radiation pattern be decomposed as:

$$\mathcal{E}_a(u) = \mathcal{E}_a^{\infty} + B_0(u-u_0) + \sum_{|\alpha|=1}^{N-1} \sum_{|\beta|=1}^{M-1} B_{\alpha,\beta}(u-u_{\alpha,\beta}), \tag{10a}$$

where $\mathcal{E}_a^{\infty} = N \times M \times \mathcal{R}(0)$ and the summation indexes satisfy $\gcd(\alpha,\beta) = 1$. The second term in Eq. (10a) is identified as the main beam radiation in the u_0 direction, which is given by:

$$B_0(u) = 2M \sum_{p=1}^{N-1} (N-p)\mathcal{R}(c^{-1}dpu). \tag{10b}$$

The summation in Eq. (10b) collectively combines the contributions with $\beta = 0$ (and therefore $|\alpha| = \pm 1$). Similarly, $B_{\alpha,\beta}$ in Eq. (10a) are the individual beam contributions, centered at the CPL direction $u_{\alpha,\beta}$:

$$B_{\alpha,\beta}(u) = \sum_{p=1}^{N_p} (N-p|\alpha|)(M-p|\beta|)\,\mathcal{R}(c^{-1}d\alpha pu), \tag{10c}$$

[§] Beams are considered here as contributing energy quantities that are centered around a prescribed direction (u) and have some spectral width.

with

$$N_p = \min\left\{\left\lfloor \frac{M-1}{|\beta|}\right\rfloor, \left\lfloor \frac{N-1}{|\alpha|}\right\rfloor\right\}. \tag{10d}$$

Due to the decaying properties of the envelope of $\mathcal{R}(\tau)$ for $|\tau| > 0$, $B_0(u)$ and $B_{\alpha,\beta}(u)$ attain their global maxima at $u = 0$ and subsequently decay away as u increases. Thus, they may be regarded as being localized around $u = 0$. Furthermore, for $B_{\alpha,\beta}$ to actually be observed in $\mathcal{E}_a$, it should have a magnitude that is greater than that of its surrounding background, i.e., according to Eq. (10a), $B_{\alpha,\beta}(0) > \mathcal{E}_a^{\infty} + B_0(u_{\alpha,\beta} - u_0) + \sum_{\alpha',\beta'} B_{\alpha',\beta'}(u_{\alpha,\beta} - u_{\alpha',\beta'})$, where $|\alpha'| = 1 \dots N-1$, $\alpha' \neq \alpha$, and $|\beta'| = 1 \dots M-1$, $\beta' \neq \beta$. In all other cases, the beams' contribution is negligible and is absorbed into the background. It should be noted that this last condition on the beam's observability depends on: (*i*) the spectral density of the beams (in u); and (*ii*) the elements' radiation pattern $|\mathbf{f}(\hat{\mathbf{r}})|^2$ via Eq. (6a).

Since the CPLs are confined within the spectral region $u_{1,-|M-1|} \leq u \leq u_{1,M-1}$, it follows that beyond this region of confinement (i.e., following (8), $|u - u_0| > (M-1)cT_p/d$), the argument of the autocorrelation functions in Eq. (10) by far outnumbers cT/d (a measure of the correlation length of $\mathcal{R}$); hence, all the beams' contributions are negligibly small, giving $\mathcal{E}_a(u) = \mathcal{E}_a^{\infty}$. For further discussion see the concluding paragraph in Section 6.

As follows from Eq. (10c), for different beam indexes (α,β), the corresponding CPLs, $B_{\alpha,\beta}(u)$, are not scaled replicas of one another (as in the similar case of GLs with TH excitation). This conclusion follows from $F_a(u_{\alpha,\beta}, \tau)$, which in view of Eq. (9) exhibits different pulsed sequences for different sets of α, β (see in [15, Fig. 2]).

Once the decomposition of $\mathcal{E}_a$ in Eq. (10) yields a concise representation in terms of the set of (α, β)-CPLs, The normalized magnitude of the array's energy radiation pattern for the different CPLs (i.e., at $u_{\alpha,\beta}$), termed the array's CPL-level (A-CPLL) is calculated:

$$\text{A-CPLL}_{\alpha,\beta} = \frac{\mathcal{E}_a(u_{\alpha,\beta})}{\mathcal{E}_a(u_0)} \simeq \frac{\mathcal{E}_a^{\infty} + B_{\alpha,\beta}(0)}{\mathcal{E}_a^{\infty} + B_0(0)} \tag{11a}$$

$$= \frac{1+2N_p}{N} + \frac{N_p(N_p+1)}{MN^2}\left\{\frac{2N_p+1}{3}|\alpha||\beta| - N|\beta| - M|\alpha|\right\}. \tag{11b}$$

The approximation in Eq. (11a) assumes that the beams are well separated, thus giving $\mathcal{E}_a(u_{\alpha,\beta}) \simeq \mathcal{E}_a^{\infty} + B_{\alpha,\beta}(0)$, and $\mathcal{E}_a(u_0) = \mathcal{E}_a^{\infty} + B_0(0) = MN^2\mathcal{R}(0)$. Approximating (11b) for the extreme cases of $M \to \infty$, and finite N yields $\text{A-CPLL}_{\alpha,\beta} \sim \frac{1}{|\alpha|} + \frac{1}{N^2}\frac{|\alpha|-1}{|\alpha|}$. Recalling

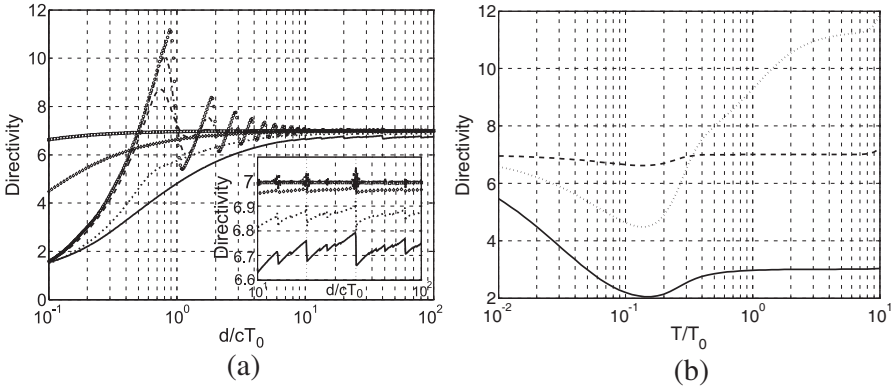

Figure 2. Directivity curves for an array with $N = 7$ elements, excited by a pulse sequence with $M = 31$ modulated pulses, $T_p/T_0 = 40$: (a) $\mathcal{D}$ as a function of the inter-element spacing d/cT_0 for different bandwidths with $T/T_0 = 0.001, 0.01, 0.1, 0.25, 0.5, 1$, and 5 ($\square$, $\diamond$, solid, dotted, dashed, dashed-dotted and $\circ$ lines, respectively); (b) $\mathcal{D}$ as a function of the frequency bandwidth for $d/cT_0 = 0.2, 0.8872$, and 10 (solid, dotted, and dashed lines, respectively).

the example in Section 4.3, the rightmost column in Table 1 lists the A-CPLL values (11), sorted by their α, β for the array. One should note the excellent agreement between the approximation obtained by (11) and the exact values shown in Fig. 1.

It should be noted that: (*i*) following Eq. (11), A-CPLL depends on the number of pulses M in the excitation signal $s(t)$; (*ii*) furthermore, in the case in which the CPLs are not well separated, one should use the exact definition in the first equality in (11a), which suggests that the temporal pulsed waveform also affects the A-CPLL via its autocorrelation in (10); and (*iii*) since the radiating elements may have a radiation pattern that is not omnidirectional (i.e., $|f(\hat{\mathbf{r}})|^2 \neq 1$), the actual $\text{CPLL}_{\alpha,\beta}$ may be lower than the $\text{A-CPLL}_{\alpha,\beta}$.

6. ARRAY SPARSITY

As follows from the above discussion, the array and excitation parameters determine the angular distribution of the radiated beams (beam skeleton, GLs, and SLs). Furthermore, the numerical values assigned to those parameters, in turn, determine the number of radiation beams within the visible spectral domain. In array design, sometimes there is a need to design arrays with as few elements as possible to meet some given radiation properties. However, as the

inter-element spacing becomes larger than some threshold, and the array becomes sparse (with respect to given measures), the design results in some additional dominant radiated beams that can cause spurious effects upon using the array in a system (e.g., remote sensing/imaging, etc.). In this section we explore this threshold and its consequent effect in view of the beam skeleton.

For this discussion, we consider a sparse array as an array whose inter-element spacing (d) is greater than some prescribed quantity ("threshold") that is associated with any periodicity inherent in the array, i.e., physical layout, pulsed sequence and microstructure of the pulsed temporal waveform. Consequently, the array's radiation pattern constitutes more than its main radiation beam (and its SLs) within the visible spectral domain (i.e., attaining, also, GLs and/or CPLs). The possible periodicities, if they do indeed exist, induced by the array's setting suggest two sparsity measures: (i) pulse repetition sparsity (PRS), i.e., sparsity with respect to the pulse repetition duration T_p (or the PRF); and (ii) sparsity with respect to the pulse's microstructure, i.e., modulation or in-pulse ripple (manifested by the τ_γ), termed microstructure sparsity (MS). The closest CPL to the main beam (u_0 direction) has $(|\alpha|,|\beta|)=(N-1,1)$; thus, in light of Eq. (8a), setting this beam outside the observation domain ($|u|>1$)suggests that $d<\left[(N-1)(1+|u_0|)\right]^{-1}cT_p$. Hence, for a PRS array, $d\geq\left[(N-1)(1+|u_0|)\right]^{-1}cT_p$. This thresholding demonstrates the effect of the excitation sequence PRF on the radiation pattern or alternatively sets design guidelines for obtaining an HPRF array free of "spurious" beam within the observation domain. On the other hand, MS is associated with the presence of main beam GLs within the visible spectral domain in QM and NB excitations, in a manner similar to the TH excitation. In that case, for an MS array, $d\geq\left[1+|u_0|\right]^{-1}|c\tau_{\pm1}|$, which suggests that there is at least one GL within the observation domain. Note that in the TH regime, where $c\tau_\gamma=\gamma cT_0=\gamma\lambda_0$ (λ_0 is the wavelength at the carrier frequency), the MS criterion coincides with the TH sparsity [30]. Furthermore, for QM (and NB) excitations, both PRS and MS may exist, but for UWB/SP excitation regime, PRS is the dominant mechanism. Obviously, as already discussed in previous work [13, 15, 24], sparse arrays can be designed such that they have some favorable properties.

To conclude this part of the paper, we note that as d grows beyond the PRS threshold more and more CPLs are driven into the visible spectral domain. The highest CPL to enter is indexed by $(|\alpha|,|\beta|)=(1,M-1)$, and the critical inter-element spacing for this to occur is $d>(M-1)\left[1+|u_0|\right]^{-1}cT_p$ (see, e.g., (8a)). Once all the CPLs are within the visible spectral domain, a further increase

in d results in the enclosure of all the CPLs within a spectral span $|u-u_0| \leq (M-1)cT_p d^{-1}$. For u outside this spectral domain, $F_a(u,\tau)$ breaks into a sequence of $N \times M$ essentially separate pulses, which yield a constant energy radiation pattern $\mathcal{E}_a(u) = \mathcal{E}_a^{\infty}$. Recall that for a single pulse excitation ($M = 1$), sparsity can be defined with respect to the breaking of the main radiation beam into a sequence of N distinct pulses. This definition suggests the criterion $d/cT > 1$ (where T is a measure of the radiated pulse) for the sparse array, see in [13, 24]. This type of sparsity may be termed pulse width sparsity (PWS). In light of this definition, the condition $d > (M-1)\left[1+|u_0|\right]^{-1} cT_p$ induces a PWS-like condition.

7. ARRAY DIRECTIVITY

Following the discussion on the radiation pattern characteristics, we now introduce directivity as a figure of merit for the array's performance and explore its properties in view of the beam skeleton. Directivity is defined here with respect to the energy radiation pattern as in TH, see Refs. [30, 31]. The aim here is to quantify the net effect of the various radiation lobes on the array's directivity. To this end, we assume that the angular radiation pattern of the radiation elements is omnidirectional, $|\mathbf{f}(\hat{\mathbf{r}})| = 1$ (hence $\mathcal{E}_a = \mathcal{E}$). Note, though, that the temporal characteristics of the elements' response are already embedded within the energy radiation pattern via the $\mathcal{R}_D$ operator in (4). Consequently, the array's directivity is given by:

$$\mathcal{D}_a = 4\pi \frac{\max_{\hat{\mathbf{r}}} \mathcal{E}_a(\hat{\mathbf{r}})}{\iint\limits_{4\pi} d\Omega\, \mathcal{E}_a(\hat{\mathbf{r}})} = 2\frac{\mathcal{E}_a(u_0)}{\int\limits_{-1}^{1} du\, \mathcal{E}_a(u)} \tag{12}$$

where $d\Omega = \sin\theta d\theta d\phi$. It is important to note that, in practice, since $f(\hat{\mathbf{r}})$ is not omnidirectional, it tends to smooth out the $\mathcal{E}_a$ term in Eq. (12) and hence to decrease the effect of the CPLs, GLs and SLs on the radiation pattern away from the array's steering direction and, consequently, the effect of the lobes on the directivity $\mathcal{D}$ (calculated using the first equality in (12) with $\mathcal{E}$ instead of $\mathcal{E}_a$).

Next, inserting the expression for the energy radiation pattern of Eq. (10) into Eq. (12) yields the array's directivity in terms of the

different beam contributions as:

$$\mathcal{D}_a = \Bigg[\frac{1}{N} + \frac{1}{N^2}\sum_{p=1}^{N-1}\frac{N-p}{p}\Gamma(p,u_0) + \frac{1}{2N^2M}\sum_{|\alpha|=1}^{N-1}\sum_{|\beta|=1}^{M-1}\sum_{p=1}^{N_p}\frac{N-p|\alpha|}{p|\alpha|}(M-p|\beta|)\Gamma(p|\alpha|,u_{\alpha,\beta})\Bigg]^{-1} \tag{13a}$$

where the summation over α and β is restricted by $\gcd(\alpha,\beta)=1$ and includes only those beams that contribute to the radiation pattern within the visible observation domain $|u_{\alpha,\beta}| \lesssim 1$ (see the discussion in item i of Section 4.2), and

$$\Gamma(l,\bar{u}) = \frac{c}{d}\int_{-(1+\bar{u})lc^{-1}d}^{(1-\bar{u})lc^{-1}d} du\ \frac{\mathcal{R}[u]}{\mathcal{R}[0]}, \tag{13b}$$

is the radiated field signal's shape factor, which may be seen as a truncated average of the signals' autocorrelation.

Expression (13) is general and can be used uniformly for calculation of the array's directivity for radiated wave fields with any bandwidth, as is discussed in the following section.

7.1. Array Directivity: Survey of Special Cases

In the following discussion, we explore several interesting, extreme (in case of parameter settings) cases to demonstrate the effect of the beam skeleton layout on the array's performance. To this end, we assume that the radiated pulsed wave-field is characterized using the effective parameters T and T_0, as was discussed after Eq. (2) (these parameters are driven from the modeling of e_0, see in (2)).

7.1.1. Time Harmonic Excitation

The first case to be discussed is the extreme NB excitation ($\frac{T}{T_0} \gg 1$) that, in view of the discussion in Section 2.1, may be identified as TH. This case may be treated by assuming that there is only a continuous modulated excitation waveform with $T_p \to \infty$. This assumption suggests that, as expected, only the main beam, with its associated SLs and GLs, lies within the visible observation domain. Furthermore, it follows that $e_0(t) \sim \cos(\omega_0 t)$, giving $\mathcal{R}(u) \sim \cos(\omega_0 u)$ for $|u| \le 1$, which in turn gives $\Gamma(p,u_0) = \frac{2}{k_0 d}\sin(pk_0 d)\cos(pk_0 d\, u_0)$, where $k_0 = \omega_0/c$

and finally

$$\mathcal{D}_a\Big|_{\text{NB}} = \left[\frac{1}{N} + \frac{2}{N^2}\sum_{p=1}^{N-1}\frac{N-p}{pk_0d}\sin\left(pk_0d\right)\cos\left(pk_0d\,u_0\right)\right]^{-1}. \qquad (14)$$

Expression (14) is the textbook result for the directivity of a linear array of N omnidirectional elements with TH excitation [30, 31].

7.1.2. Dense Array

It may easily be seen that for a dense array, where $d/cT \ll 1$ (and practically $d/cT \to 0$), i.e., the inter-element spacing is small compared to the effective pulsed width, the carrier wavelength, and the pulse repetition duration (see in Section 6), there are no CPLs within the observation domain. Eq. (13b), then, gives $\Gamma(l, \bar{u}) \approx 2l$ to yield $\mathcal{D}_a \simeq 1$ (similar to the case of small-sized arrays in TH antenna theory that have an omnidirectional radiation pattern [30, 31]).

7.1.3. Sparse Array

For UWB/SP excitation, the radiated pulse consists of a small number of cycles, possibly less than one, such that $e_0(t)$ is set to yield a "nice enveloped/bell-shaped" pulse. In that case, let the correlation length (width of $\mathcal{R}$) be linearly proportional to T. For a large enough d/cT (usually > 1, near or beyond the range of d for sparse array realization), the integration limits in Eq. (13b) may be altered to approximate Γ by:

$$\Gamma(p|\alpha|, u_{\alpha,\beta}) \simeq \frac{c}{d}\mathcal{H}(1 - |u_{\alpha,\beta}|)\int_{-\infty}^{\infty} dy\,\frac{\mathcal{R}[y]}{\mathcal{R}[0]}, \qquad (15)$$

where $\mathcal{H}(\cdot)$ is the Heaviside step function. Inserting Eq. (15) into Eq. (13a) yields the final expression for the directivity of the UWB/SP driven array. Moreover, since the correlation length depends linearly on T, it follows according to (13b), that $\Gamma(p|\alpha|, u_{\alpha,\beta}) \sim \frac{cT}{d}$. Consequently, sparse conditions with $\frac{d}{cT} \gg 1$ give rise to $\mathcal{D} \to N$ (see also Fig. 2(a)).

7.2. Array Directivity: Example

To conclude the discussion in this section, we provide an example to demonstrate the above concepts of directivity and its performance for the different cases of Section 7.2.

The first example (Fig. 2) depicts the directivity curves of an array with $N = 7$ elements, excited by a pulse sequence with $M = 31$

Gaussian modulated pulses (e_0 as in Section 4.3), $T_p/T_0 = 40$ where T_0, the carrier period, is used for normalization, see the discussion in Section 2.1, and $u_0 = 0$. Fig. 2(a) shows $\mathcal{D}$ as a function of the inter-element spacing d/cT_0 for different wave-field frequency bandwidths with $T/T_0 = 0.001, 0.01, 0.1, 0.25, 0.5, 1$ and 5. Here, $\mathcal{D}$ was calculated by Eq. (12). Note that the span of d/cT_0 covers the conditions for MS (NB and QM excitations) and PRS (QM and UWB/SP excitations). It can be seen that for the NB regime ($T/T_0 = 5$) $\mathcal{D}$ follows the directivity curves obtained in the literature for the classical TH antenna theory, which is given by Eq. (14) [31]. As the bandwidth is increased from NB to QM regimes, by lowering T/T_0, the smooth undulations of $\mathcal{D}$, due to the GL dynamics within the observation domain, decay to somewhat low values as $d/cT_0 \sim \mathcal{O}(1)$. A further increase in the frequency bandwidth toward the UWB/SP regime ($T/T_0 = 0.25, 0.1, 0.01$, and 0.001) introduces a new type of "staircase"-like oscillations for some high values of d/cT_0, which are attributed to CPL dynamics (see the inset in Fig. 2(a)). Fig. 2(b) depicts $\mathcal{D}$ as a function of the frequency bandwidth for $d/cT_0 = 0.2, 0.8872$, and 10. As can be seen, $\mathcal{D}$ attains its minimum value for $T/T_0 \simeq 0.14$, which may be identified as the transitional point between UWB/SP and QM bandwidth regimes. This minimum in $\mathcal{D}$ may be attributed to the fact that $e_0(t)$ is obtained as an interplay between two temporal waveforms, a pulsed envelope ($r(t)$), which is dominant for $T/T_0 \lesssim 0.14$, i.e., less than one cycle signal, and the carrier cosine $\cos\omega_0 t$, which is dominant for $T/T_0 \gtrsim 0.14$.

In the second example (Fig. 3), $\mathcal{D}$ is shown as a function of d/cT for an array with $N = 7$ elements, excited by a pulse sequence that is modeled as in the previous examples, where $T = 1$, $T_p/T = 45$, $T/T_0 = 0.1$ (UWB/SP regime), and the number of modulated pulses is $M = 2$, 5, 15, and 35, and $u_0 = 0$. It can be seen that as the number of pulses increases, the array's directivity becomes lower, since the radiated energy tends to disperse between an increased number of CPLs. Moreover, whenever a new CPL "enters" the visible domain, an abrupt drop in $\mathcal{D}$ is observed, which may be seen in Fig. 3 from the staircase-like behavior of the curves. Furthermore, once $d/cT_p \geq (M-1)$, all the CPLs are already within the observation domain, while a further increase in d/cT only "squeezes" the CPL skeleton more and more towards the main beam, and the array is now in its PWS condition (recall the discussion in Section 6). Furthermore, in this condition, there is a smooth increase in the array's directivity due to the decrease in the span of the radiated beams ("beam squeezing"). The $\circ$ markings on the $M = 5$ curve that overlap indistinguishably with the dotted line of the curve denote the approximated directivity calculated by using Eq. (13a) with Eq. (15).

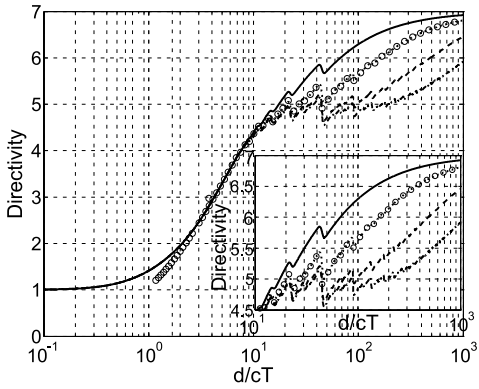

Figure 3. $\mathcal{D}$ as a function of d/cT for an array with $N = 7$ elements, excited by a pulse sequence, where $T = 1$, $T_p/T = 45$, $T/T_0 = 0.1$ and the number of pulses is $M = 2, 5, 15$, and 35 (solid, dotted, dashed, and dashed-dotted lines, respectively). The small circle markings over the $M = 5$ (dotted) line represent the directivity as calculated by using the approximation in (15).

Note that the approximation becomes valid for $d/cT > 1$ (see the discussion in Section 7.1.3). Furthermore, the approximation is sufficiently accurate, except for $d/cT \simeq (|\beta|/|\alpha|)(T_p/T)$, i.e., in the immediate vicinity of the abrupt drops in $\mathcal{D}$ (as may be seen in the inset in Fig. 3 for the indistinguishable curves for $M = 5$). These values of d/cT correspond to the rise of a new CPL within the visible spectral domain ($u_{\alpha,\beta} = 1$). Possible inaccuracies observed in the approximation in the vicinity of the abrupt changes in $\mathcal{D}$ are due to the augmentation of the finite integration limits in Eq. (13b) to infinite limits in Eq. (15), which implies that there are no partial CPL contributions within the visible domain, i.e., the use of Eq. (15) implies that whenever a new CPL appears, it immediately contributes its full effect to decreasing $\mathcal{D}$. This assumption stands in contrast to the physical realization that the CPLs gradually enter the visible domain as d/cT increases.

8. CONCLUSION

The kinematic properties of a sparse TTD beam steering array radiating a possibly modulated-like periodic pulsed sequence were explored. The TD radiation pattern was introduced as an intermediate step in formulating the energy radiation pattern. Since the energy pattern is time independent but nevertheless encapsulates the basic kinematic properties of the array, it serves for characterization of the

array. Next, the beam (radiation lobes) skeleton was introduced as the set of all radiation directions for which there are local angular energy peaks (or alternatively a cross pulsed coherent interference in TD). These energy peaks were identified as CPLs and GLs. GLs are common in QM and NB excitation regimes, while CPLs are a basic property of periodic pulsed excitation. The lobe/beam skeleton led to the decomposition of the energy pattern into a summation of beam contributions that are angularly centered around the CPLs' directions. The beam skeleton depends on the array parameters, i.e., inter-element spacing, effective pulse width, carrier period (if a modulated pulse is indeed used or approximated), and the excitation sequence PRF. In light of these array parameters, the sparsity of the array was addressed, where a sparse array constitutes a radiation field (radiation pattern) with more than one beam within the observation domain (the main beam and at least one GL or CPL). Hence, the PRS was defined as the condition of having CPLs within the observation domain, while MS was defined as the condition of having no CPLs but only GLs within the observation domain. Having discussed the kinematic properties of the array, we presented the array's directivity as a figure of merit for its performance. The derived expression for the directivity can be used uniformly with excitation signals within the three bandwidth regimes. Moreover, for NB excitation, it gives rise to the expression known from classical array theory under TH excitation. For QM and UWB/SP types of excitations, the directivity is also affected by CPLs (beam skeleton properties) within the visible radiation domain. For the range of parameters used in the present demonstrations, a regular behavior of the directivity was observed. Different setting of the parameters and in particular an interplay between the element's spatial distribution, the single pulse waveform and the pulse sequence may lead to an extreme state of the directivity in the form of super-directivity. This issue is explored elsewhere with regard to array synthesis and optimization.

In conclusion, let us consider three further points: (*i*) The discussion here assumed a unidimensional array, but it can also be extended, following the same arguments of derivation, to 2- and 3-dimensional arrays, where the radiation pattern depends on two spectral parameters, i.e., $u = \cos\theta\cos\phi$ and $v = \cos\theta\sin\phi$. (*ii*) The present characterization shows that the TH kinematic antenna theory (SL, GL, directivity and sparsity) is a special case of the time-dependent array under periodic pulsed excitation. (*iii*) The present discussion may be viewed as divided into two parts. In the first part, a mathematical formulation of the ERP, the beam skeleton and the various beam types was introduced. The second part used the ERP formulation to discuss the array sparsity and the directivity. Once

the characteristics of the sparsity and directivity were identified they can be used for further analysis/synthesis and optimization of the array performance. Note that synthesis or optimization of the array performance can be carried out with respect to other parameters either in the TD pattern or in the energy pattern (ERP). Nevertheless the present discussion shows that TD characteristics are also manifested in the ERP. Hence, kinematic optimization with respect to various parameters (other than the directivity and sparsity) can be formulated with the ERP. Moreover, the present discussion assumed an ERP that is expressed via the $\mathcal{L}_2$ norm (3), but a similar analysis can be performed for any $\mathcal{L}_p$ norm (see, e.g., the numerical example for the ∞ norm in [15, Figure 5]) or norms that are defined over finite temporal duration. Thus emphasizing additional TD characteristics that may also be synthesized or optimized. Finally, in TTD arrays such as those discussed here, one may optimized the performance with respect to three sets of degrees of freedom: the array spatial distribution (d), the single pulse characteristics (T, T_0), and the excitation sequence (T_p). These issues are being pursued elsewhere.

ACKNOWLEDGMENT

This research was supported by The Israel Science Foundation (Grant No. 745/07).

REFERENCES

1. Stepanishen, P. R., "The transient response of arrays of transducers," *Journal of the Acoustical Society of America*, Vol. 50, No. 3, 964–974, 1971.
2. Bertoni, H. L., L. Carin, and L. B. Felsen, *Ultrawideband/Short-pulse Electromagnetics*, Vol. 1, Plenum Press, New York, 1993.
3. Carin, L. and L. B. Felsen, *Ultrawideband/Short-pulse Electromagnetics*, Vol. 2. Plenum Press, New York, 1995.
4. Baum, C. E., L. Carin, and A. P. Stone, *Ultrawideband/Short-pulse Electromagnetics*, Vol. 3. Plenum Press, New York, 1997.
5. Baum, C. E., *General Properties of Antennas*, No. 330, Sensor and Simulation Notes, 1991.
6. Baum, C. E. and E. G. Farr, *Extending the Definitions of Antennas Gain and Radiation Pattern into the Time Domain*, No. 350, Sensor and Simulation Notes, 1992.
7. Shlivinski, A., E. Heyman, and R. Kastner, "Antenna characterization in the time domain," *IEEE Trans. Antennas Propagat.*, Vol. 45, 1140–1149, Jul. 1997.

8. Hernandez, J. E., R. W. Ziolkowski, and S. R. Parker, "Synthesis of the driving functions of an array for propagating localized wave energy," *Journal of the Acoustical Society of America*, Vol. 92, 550–562, Jul. 1992.
9. Ziolkowski, R. W., "Properties of electromagnetic beams generated by ultra-widebandwidth pulse-driven arrays," *IEEE Trans. Antennas Propagat.*, Vol. 40, No. 8, 888–905, 1992.
10. Baum, C. E. and E. G. Farr, *Timed Arrays for Radiating Impulse-like Transient Fields*, No. 361, Sensor and Simulation Notes, 1993.
11. Murino, V., A. Trucco, and A. Tesei, "Beam pattern formulation and analysis for wide-band beamforming systems using sparse arrays," *Signal Processing*, Vol. 56, 177–183, 1997.
12. McGrath, D. T. and C. E. Baum, "Scanning and impedance properties of TEM horn arrays for transient radiation," *IEEE Trans. Antennas Propagat.*, Vol. 47, No. 3, 469–473, 1999.
13. Schwartz, J. L. and B. D. Steinberg, "Ultrasparse, ultrawideband arrays," *IEEE Transactions on UFFC*, Vol. 45, 376–393, Mar. 1998.
14. Cardone, G., G. Cincotti, P. Gori, and M. Pappalardo, "Optimization of wide-band linear arrays," *IEEE Transactions on UFFC*, Vol. 48, 943–952, Jul. 2001.
15. Shlivinski, A. and E. Heyman, "A unified kinematic theory of transient arrays," *Ultra-wideband, Short-pulse Electromagnetics*, P. Smith and S. R. Cloude, Eds., Vol. 5, 11–20, Plenum Press, NY, 2002.
16. Shlivinski, A. and E. Heyman, "Discrete array representation of continuous space-time source distributions," *Turk. J. Elec. Engin.*, Vol. 10, No. 2, 257–271, 2002.
17. Curletto, S., C. Parodi, and A. Trucco, "On the stability of wideband beam patterns with respect to weighting and envelope fluctuations," *Ultrasonics*, Vol. 42, No. 1–9, 997–1003, 2004.
18. Franceschetti, G., J. Tatoian, and G. Gibbs, "Timed arrays in a nutshell," *IEEE Trans. Antennas Propagat.*, Vol. 53, No. 12, 4073–4082, 2005.
19. Sörgel, W., C. Sturm, and W. Wiesbeck, "Impulse responses of linear UWB antenna arrays and the application to beam steering," *Proc. of the IEEE International Conference on Ultra-wideband, ICU 2005*, 275–280, Sep. 2005.
20. Curletto, S. and A. Trucco, "On the shaping of the main lobe in wide-band arrays," *IEEE Transactions on UFFC*, Vol. 52, 619–630, Apr. 2005.

21. Wang, Q., N. Guo, H. Du, and W. Huang, "Beam pattern calculation for optimization of broadband array transducers," *Journal of the Acoustical Society of America*, Vol. 120, No. 2, 741–749, 2006.
22. Ries, S. and T. Kaiser, "Ultra wideband impulse beamforming: It is a different world," *Signal Processing*, Vol. 86, No. 9, 2198–2207, 2006.
23. Ciattaglia, M. and G. Marrocco, "Investigation on antenna coupling in pulsed arrays," *IEEE Trans. Antennas Propagat.*, Vol. 54, 835–843, Mar. 2006.
24. Hussain, M. G. M. and A. S. Al-Zayed, "Aperture-sparsity analysis of ultrawideband two-dimensional focused array," *IEEE Trans. Antennas Propagat.*, Vol. 56, 1908–1918, Jul. 2008.
25. Ciattaglia, M. and G. Marrocco, "Time domain synthesis of pulsed arrays," *IEEE Trans. Antennas Propagat.*, Vol. 56, 1928–1938, Jul. 2008.
26. Shlivinski, A. and E. Heyman, "Time-domain near-field analysis of short-pulse antennas — Part I: Spherical wave (multipole) expansion," *IEEE Trans. Antennas Propagat.*, Vol. 47, No. 2, 271–279, 1999.
27. Marrocco, G. and G. Galletta, "Hermite-rodriguez UWB circular arrays," *IEEE Trans. Antennas Propagat.*, Vol. 58, 381–390, Feb. 2010.
28. Stepanishen, P. R., "Pulsed transmit/receive response of ultrasonic piezoelectric transducers," *Journal of the Acoustical Society of America*, Vol. 69, No. 6, 1815–1827, 1981.
29. Cheng, D. K. and F. I. Tseng, "Transient and steady state antenna pattern characteristics for arbitrary time signals," *IEEE Trans. Antennas Propagat.*, Vol. 12, 492–493, 1964.
30. Balanis, C. A., *Antenna Theory: Analysis and Design*, 3rd edition, Wiley-Interscience, 2005.
31. Stutzman, W. L. and G. A. Thiele, *Antenna Theory, and Design*, 2nd Edition, John Wiley & Sons, Inc., 1998.
32. Compton, Jr., R. T., "The bandwidth performance of a two-element adaptive array with tapped delay-line processing," *IEEE Trans. Antennas Propagat.*, Vol. 36, 5–14, Jan. 1988.
33. Vook, F. W. and R. T. Compton, Jr., "Bandwidth performance of linear adaptive arrays with tapped delay-line processing," *IEEE Transactions on Aerospace Electronic Systems*, Vol. 28, 901–908, Jul. 1992.